Design of magnetic spirals in layered perovskites: extending the stability range far beyond room temperature

Tian Shang[1,2,3*], Emmanuel Canévet[4,5], Mickaël Morin[1,6], Denis Sheptyakov[4], María Teresa Fernández-Díaz[7], Ekaterina Pomjakushina[1], and Marisa Medarde[1,*]

[1] Laboratory for Multiscale Materials Experiments,

Paul Scherrer Institut, CH-5232 Viligen PSI, Switzerland

[2] Swiss Light Source,

Paul Scherrer Institut, CH-5232 Viligen PSI, Switzerland

[3] Institute of Condensed Matter Physics,

École Polytechnique Fédérale de Lausanne (EPFL), CH-1015 Lausanne, Switzerland

[4] Laboratory for Neutron Scattering and Imaging,

Paul Scherrer Institut, CH-5232 Viligen PSI, Switzerland

[5] Department of Physics, Technical University of Denmark, 2800 Kgs. Lyngby, Denmark

[6] Excelsus Structural Solutions (Swiss) AG

PARK innovAARE, CH-5234, Villigen, Switzerland

[7] Institut Laue Langevin,

71 avenue des Martyrs, CS 20156 -38042 Grenoble CEDEX 9, France

*Corresponding authors (tian.shang@psi.ch; marisa.medarde@psi.ch)

Abstract

In insulating materials with ordered magnetic spiral phases, ferroelectricity can emerge due to the breaking of inversion symmetry. This property is of both fundamental and practical interest, in particular with a view to exploiting it in low-power electronic devices. Advances towards technological applications have been hindered, however, by the relatively low ordering temperatures T_{spiral} of most magnetic spiral phases, which rarely exceed 100 K. We have recently established that the ordering temperature of a magnetic spiral can be increased up to 310 K by the introduction of chemical disorder. Here we explore the design space opened up by this novel mechanism by combining it with a targeted lattice control of some magnetic interactions. In Cu-Fe layered perovskites we obtain T_{spiral} values close to 400 K, comfortably far from room temperature and almost 100 K higher than using chemical disorder alone. Moreover, we reveal a linear, universal relationship between the spiral's wave vector and the onset temperature of the spiral phase. This linear law ends at a paramagnetic-collinear-spiral triple point, which defines the highest spiral ordering temperature that can be achieved in this class of materials. Based on these findings, we propose a general set of rules for designing magnetic spirals in layered perovskites using external pressure, chemical substitutions and/or epitaxial strain, which should guide future efforts to engineer magnetic spiral phases with ordering temperatures suitable for technological applications.

Introduction

Magnetic frustration is characterized by the magnetic interactions that cannot be simultaneously satisfied[1, 2, 3, 4, 5, 6] and may lead to non-trivial magnetic orders[7, 8, 9, 10, 11]. An example of such exotic magnetically ordered phases is the spin spiral, which has received a lot of attention during the last decade due to its potential for inducing ferroelectricity in insulating materials[12, 13, 14, 15, 16]. A necessary condition to use this property for magnetoelectric applications is to stabilize the spiral state close to room temperature (RT). Unfortunately, very few insulators display spiral phases above 100 K.

Besides cupric oxide (CuO) and some hexaferrites [17, 18, 19, 20], the layered perovskite $YBaCuFeO_5$ is one of the few exceptions to this rule. However, what makes this last material truly remarkable is the extraordinary tunability of its spiral ordering temperature (T_{spiral}), which can be increased by more than 150 K by manipulating the degree Cu/Fe chemical disorder in the structure. We showed recently that T_{spiral} can be shifted from 154 K to 310 K by adjusting the average Cu/Fe occupations n_{Cu} and n_{Fe} of the square-pyramidal sites in the crystal unit cell (Fig. 1A) [21]. We also established the existence of a positive correlation between the spiral ordering temperature and the degree of Cu/Fe intermixing (maximal for $n_{Cu} = n_{Fe} = 50\%$). However, the most surprising observation was that tiny differences in the Cu/Fe occupations ($|n_{Cu} - n_{Fe}| \leq 6\%$) can shift T_{spiral} by more than 150 K. Such a huge, positive impact of the Cu/Fe disorder in the spiral stability is remarkable, and calls for further investigations aimed to both, understanding and exploiting this unusual trend.

The aim of the present study is to explore the design space opened by this novel, disorder-based spiral control mechanism. After having shown its potential and limitations for the particular case of YBaCuFeO$_5$[21], we combine it here with a targeted lattice tuning of some magnetic exchanges. The idea behind is to add-up the effect of both mechanisms in order to stabilize spin spirals at temperatures higher than those obtained using these two strategies separately. In the following we show that for Cu-Fe based layered perovskites, T_{spiral} values close to 400 K can be obtained using this approach. These values are ~100 K higher than using chemical disorder alone[21], and expand the stability range of the spiral to a comfortable temperature region that extends well beyond RT. We also uncover the existence of an intriguing paramagnetic–collinear-spiral triple point which defines the highest T_{spiral} value that can be achieved in this class of materials. Moreover, we find several correlations between the spiral properties and some structural parameters that can be summarized in the form of a simple set of rules for magnetic spiral design in layered perovskites. Besides overcoming limiting factors in terms of operating temperatures, these results could contribute to increase the number of materials featuring spiral phases stable well beyond RT and be an important step towards the technological application of magnetic spirals in spintronics devices.

Results

Magnetic interactions

The strategy followed to attain our goal is based in the particularities of the YBaCuFeO$_5$ crystal structure and the associated nearest-neighbor (NN) exchange couplings. A

4

schematic representation of the layered perovskite unit cell of this material (space group *P4mm*) is shown in Fig. 1A[22, 23, 24]. The A-sites are occupied by equal amounts Y^{3+} and Ba^{2+} which order in planes perpendicular to the *c*-axis owing to their very different ionic radii[25]. The B sites host Fe^{3+} and Cu^{2+} in square-pyramidal coordination that form slabs of 'bowties' separated by Y^{3+} layers. Contrarily to Y and Ba, Cu and Fe display a very particular kind of correlated disorder which is characterized by the preferential occupation of the bowties by Cu-Fe pairs[24]. Such Cu-Fe 'dimers' are disordered in the structure (see Fig. 1B), leading to variable, preparation-dependent averaged Cu/Fe occupations of the atomic positions inside the pyramids.

The Cu-Fe dimers have very important consequences for the magnetism of $YBaCuFeO_5$. As demonstrated in refs. 24, 26, all possible in-plane NN interactions J_{ab} (Fe-Fe, Cu-Cu and Cu-Fe) are strong and antiferromagnetic (AFM), see Fig. 1B. J_{c1}, one of the two NN couplings along *c*-axis (Fig. 1C) is also AFM and disorder-independent, but its value is about one order of magnitude smaller. The intra-bowtie coupling J_{c2}, comparable to J_{c1} in absolute value, is the only ferromagnetic (FM) NN exchange interaction, and it is worth noting that this is only possible if the bowties are preferentially occupied by Cu-Fe pairs (i.e., if $J_{c2} = J_{Cu-Fe}$)[24]. This set of magnetic interactions is at the origin of the collinear magnetic phase observed at high temperatures ($T < T_{collinear}$) with $\mathbf{k_c} = (½ \ ½ \ ½)$, see Fig. 1C[21, 24, 27, 28, 29, 30]. Note that in spite of the underlying chemical disorder, the preferential occupation of the bowties by FM Cu-Fe dimers and the non-dependence of the sign of J_{ab} and J_{c1} with the Cu/Fe disorder imply that the magnetic structure can be seen as a set of *ordered* layers with strong in-plane AFM bonds coupled though weak, alternating FM and AFM bonds along *c*-axis (Fig. 1D).

At low temperatures the k_z component of the propagation vector becomes incommensurate and the collinear magnetic order transforms in an inclined circular spiral with $\mathbf{k_i}$ = (½ ½ ½±q) (Fig. 1E)[21, 24, 28, 29, 31]. Although the **c**-axis seems naturally more prone to a magnetic instability due the weakness of J_{c1} and J_{c2}, the appearance of spiral state is surprising because these two couplings are not frustrated, and the next-nearest-neighbor (NNN) interactions, estimated from DFT calculations, are either too small, or have the wrong sign to produce frustration along this direction[24, 26, 32, 33].

Tuning T_{spiral} with chemical disorder

Very recently, an alternative, disorder-based mechanism has been proposed by Scaramucci and co-workers [32]. These authors demonstrated that a magnetic spiral can be stabilized through the introduction of few strong, randomly distributed frustrating bonds in systems featuring a *single* crystallographic direction with weak NN magnetic couplings. $YBaCuFeO_5$, with strong in-plane couplings and weak, alternating AFM/FM exchanges along **c** (Fig. 1B), clearly fulfills these premises[24, 26]. The required frustrating bonds are provided by small, preparation-dependent amounts of bowties occupied by Fe-Fe pairs (accompanied by the same amounts of Cu-Cu pairs if we assume a constant Cu/Fe ratio). Although both are energetically unfavorable[24], their presence at very low concentrations cannot be disregarded in real materials. Rather, the monotonic changes in the size of the bowties with increasing cooling rates suggest that their concentration could be directly linked to the degree of Cu/Fe disorder. Due to the small Cu^{2+} moment (S = ½) and the extremely weak Cu-Cu coupling (J_{Cu-Cu} ~ 0) (dashed-bonds in Fig. 1D), a Cu-Cu defect is expected to have only a minor impact in the

alignment of the neighboring spins. However, an AFM Fe-Fe pair (S = 5/2, J_{Fe-Fe} ~ -100 meV) (solid-green bonds In Fig. 1D) constitutes an extremely strong local perturbation of the underlying collinear spin order, in particular along the c where the couplings are weak. Such perturbation can extend to several unit cells (Fig. 1B,D), become collective and give rise to a spiral if i) the Fe-Fe defects do not cluster within the ab-plane, i.e., if they are separated by a minimal average distance ξ_{min}, ii) the J_{Cu-Fe} / J_{Fe-Fe} ratio is small enough and negative in order to guarantee strong local frustration, and iii) the concentration of Fe-Fe defects n is low enough so as to avoid that impurity bonds dominate the order between successive planes ($n < J_{Cu-Fe} / J_{Fe-Fe}$)[32, 33].

The main prediction of this model is that $both$, the spiral ordering temperature T_{spiral} and the magnetic modulation vector q should increase linearly with n, as long as it remains at such low levels[32]. Interestingly, this is qualitatively verified in $YBaCuFeO_5$ samples prepared with different cooling rates, where the highest q and T_{spiral} values are observed for the samples quenched in liquid nitrogen (i.e., those with the largest Cu/Fe disorder and where n is expected to be the highest, see Fig. 2A)[21]. It also suggests that the spiral ordering temperature could be further increased if values of n slightly larger could be achieved. Since faster cooling rates are not easily achieved experimentally, we explore here an alternative strategy based in the combination of the highest possible Cu/Fe chemical disorder with a targeted lattice tuning of some magnetic exchanges.

Adding the effect of the lattice

Based in the previous discussion, the main candidates to influence the degree of magnetic frustration at constant Cu/Fe disorder are the NN couplings J_{c1} and J_{c2} along

7

the *c*-axis, that we expect to display a negative correlation with the variation of the inter-bowtie separation (d_1) and the bowtie size (d_1), respectively (Fig. 1C)[21]. Since large changes in these two interatomic distances can be achieved through isovalent A-cation substitutions, we prepared two series of layered perovskites aimed to tune them separately. In the first one Y^{3+} was replaced by trivalent 4f cations Re^{3+} with growing ionic radius (Re_{ionic}) with the purpose of acting on d_1 (Re = Lu to Dy); in the second, Ba^{2+} was partially substituted by different amounts of smaller Sr^{2+} ($0 \leq x \leq 0.5$) with the aim of tuning d_2. In order to add-up the impact of both, the lattice and the Cu/Fe disorder, this last parameter was maximized in all the samples, which were quenched in liquid nitrogen after the last annealing (see Materials and methods section).

The impact of such d_1-tuning on T_{spiral} is illustrated in Fig. 2B, which also shows the evolution of $T_{collinear}$ with the rare earth ionic radius in the $ReBaCuFeO_5$ series as determined from powder neutron diffraction (PND). The presence of the collinear and spiral phases in all samples was confirmed by the observation of magnetic Bragg reflections corresponding to $\mathbf{k_c} = (\frac{1}{2} \frac{1}{2} \frac{1}{2})$ and $\mathbf{k_i} = (\frac{1}{2} \frac{1}{2} \frac{1}{2} \pm q)$ (Figs. 2D-E, figs. S1 and S2). The two transition temperatures change monotonically with Re_{ionic} and display completely opposite behaviors, with $T_{collinear}$ decreasing and T_{spiral} increasing for larger ionic radii. The lowest spiral ordering temperature corresponds to $LuBaCuFeO_5$ (213 K), and the highest to $DyBaCuFeO_5$ (312 K). This last value, the only one above RT (39 ºC), is 2 degrees higher that the T_{spiral} reported in ref. 21 for quenched $YBaCuFeO_5$ (Fig. 2A).

The manipulation of d_2 has also a strong impact in both transition temperatures. This is illustrated in Fig. 2C, where the evolution of $T_{collinear}$ and T_{spiral} in the $YBa_{1-x}Sr_xCuFeO_5$

family as a function of the Sr-content x is shown. PND measurements confirmed again the existence of collinear and spiral phases with propagation vectors $\mathbf{k_c}$ = (½ ½ ½) and $\mathbf{k_i}$ = (½ ½ ½±q) in all the materials investigated (Figs. 2F-G, figs. S1 and S2). We note that, contrarily to the predictions of ref. 26, $T_{collinear}$ decreases with x. T_{spiral} displays the opposite behavior, reaching 375 K (102 ºC) for x = 0.4. Linear extrapolation indicates that both temperatures should merge at ~ 395 K for x ~ 0.49, giving rise to a paramagnetic-collinear-spiral triple point. For x = 0.5, i.e., just after this point, the sample enters into a different regime characterized by an abrupt change in the stability of the spiral state. As shown in Figs. 2F and S3, the magnetic reflections associated to the propagation vector $\mathbf{k_i}$ = (½ ½ ½±q) are still present, but they are extremely weak. Moreover, they coexist with a new, very strong reflection corresponding to the propagation vector $\mathbf{k_{c'}}$ = (½ ½ 0) and those of the $\mathbf{k_c}$ = (½ ½ ½) collinear phase. These observations suggest that the spiral state is abruptly suppressed and replaced by a new antiferromagnetic phase beyond the crossing of the $T_{collinear}$ and T_{spiral} lines.

The temperature dependence of q for the $ReBaCuFeO_5$ and $YBa_{1-x}Sr_xCuFeO_5$ series together with that of $YBaCuFeO_5$ prepared using different cooling rates[21] are shown in Figs. 3A-C. For the samples with the lowest T_{spiral} we observe a smooth, continuous decrease of q characteristic of second-order phase transitions. Such behavior is progressively replaced by an abrupt collapse of q in the samples with higher T_{spiral}, suggesting that the collinear-to-spiral transition changes from second- to first-order by approaching the T_{spiral} = $T_{collinear}$ point (fig. S3). The evolution of the spiral plane inclination (φ_G) and the q value (q_G) at 10 K is shown in Figs. 3D-F. For the three series of samples we observe a clear, positive correlation among T_{spiral}, φ_G and q_G. In each family the highest T_{spiral} is observed for the sample with the largest φ_G, which reaches

values close to 90º for Re = Dy. This corresponds to a perfect cycloid, indicating that the samples with the highest spiral ordering temperature have the potential of displaying the largest saturation polarization[15, 16]. Establishing if this is the case is out of the scope of this study and will require further experimental and theoretical work.

An interesting observation, common to all the samples investigated in this study, is the existence of a linear, universal relationship between the ordering temperature and the ground state periodicity of the spiral. This can be better appreciated in Fig. 4, where the evolution of T_{spiral} with q_G for the three series of samples is shown. We note that the extrapolation of the linear law towards low-T_{spiral} values crosses the origin (i.e. $T_{collinear}$ = 0 for q_G = 0), whereas in the high-q_G side, $T_{collinear}$ and T_{spiral} converge to a common value of ~ 395 K for q_G ~ 0.18. The sudden disappearance of the spiral and the observation of a new magnetic phase close to this point suggest the existence of a limiting value for *both,* the spiral's periodicity and ordering temperature. In other words, 395 K is most probably the *highest* T_{spiral} value that can be reached in Cu-Fe-based layered perovskites. To our best knowledge, it is the highest spiral ordering temperature reported for a transition metal oxide[34]. Moreover, it is comfortably far from room temperature, an important point regarding applications, and almost 100 K higher than the highest T_{spiral} value previously reported for $YBaCuFeO_5$ using chemical disorder alone (310 K).

Chemical disorder versus lattice tuning

After demonstrating the success of our combined approach, we investigate in detail the associated changes in the crystal structure with the aim to getting additional insight on

their link with the degree of magnetic frustration. We employ high resolution PND (fig. S6) to obtain precise values of the different structural parameters for the ReBaCuFeO$_5$ and YBa$_{1-x}$Sr$_x$CuFeO$_5$ series, that we compare with those obtained for YBaCuFeO$_5$ prepared using different cooling rates[21]. We check first the average Cu/Fe occupancies n_{Cu} and n_{Fe} of the bipyramidal sites, that we expected to be very similar owing to the quenching procedure used during the synthesis. The obtained values, shown in Figs. 5A-C and tables S3-6, confirm a high degree of disorder in all samples, which display average Cu/Fe occupancies very close to 50%.

The evolution of the lattice parameters and the tetragonal distortion $c/2a$ for the three series are summarized in Figs. 5D-L. Based in the results obtained for YBaCuFeO$_5$ prepared with different degrees of Cu/Fe disorder, we established in ref. 21 an empirical, positive correlation between $c/2a$ and T_{spiral}, and suggested the use of this parameter for T_{spiral}-control purposes. Although a similar correlation wss observed for the ReBaCuFeO$_5$ series (Fig. 5K), Fig. 5L reveals the opposite behavior in the Sr-substituted family. This suggests that the use of $c/2a$ for the control of magnetic frustration, of potential interest in thin film growth, cannot be generalized to all Cu/Fe layered perovskites.

The modification of the inter- and intra-bowtie distances d_1 and d_2 along the c-axis and their ratio d_1/d_2 for the three series are summarized in Figs. 5M-U. The longest d_1 and shortest d_2 values are systematically observed in the three families for the samples with the highest T_{spiral} and lowest $T_{collinear}$ values. Moreover, the d_1/d_2 ratio displays a positive correlation with the spiral ordering temperature in the three series. This common

behavior indicates that, contrarily to $c/2a$, the d_1/d_2 ratio is a good parameter for the control of magnetic frustration in Cu/Fe-based layered perovskites.

In spite of a common positive correlation between T_{spiral} and d_1/d_2 ratio, Fig. 5 unravels the existence of large differences among the structural modifications in the three series. The smallest changes in the lattice parameters and the interatomic distances correspond to the $YBaCuFeO_5$ samples with different degree of Cu/Fe disorder. Interestingly, such tiny variations give raise to changes in T_{spiral} of more than 150 K, much larger than in the $ReBaCuFeO_5$ (~100 K) and $YBa_{1-x}Sr_xCuFeO_5$ (~90 K) series where the variation of the lattice parameters and interatomic distances is much more pronounced. This is better appreciated in Fig. 5V, where the evolution of T_{spiral} and with d_1/d_2 is displayed. This parameter, which reflects the relative strength J_{c2}/J_{c1} of the couplings along the c-axis, changes very little in the $YBaCuFeO_5$ samples with different degree of disorder (0.41%). However, it increases by more than 1.7% between the two extremes of the $YBa_{1-x}Sr_xCuFeO_5$ family, and by 4.6% in the $ReBaCuFeO_5$ series. These results confirm the exceptional efficiency of chemical disorder alone for T_{spiral} tuning. On the other side, our data show also that a comparable efficiency in terms of T_{spiral} increase can be reached at fixed degree of chemical disorder by acting *exclusively* on the lattice. A particularly interesting observation is that the impact of both mechanisms on the spiral ordering temperature is additive: once the highest T_{spiral} value is reached by manipulating the Cu/Fe disorder, it can be further increased through the maximization of the d_1/d_2 ratio. This allows T_{spiral}-tuning over unprecedentedly large temperature ranges, providing at the same time versatile tool for stabilizing spin spirals at temperatures well beyond RT.

Experiment versus theory

Having presented the experimental facts, we compare now our observations with the predictions of the random frustrating bonds (RFB) model proposed by Scaramucci and co-workers[32, 33]. The main prediction of this model is that both, T_{spiral} and q should increase with the concentration of Fe-Fe frustrating bonds n. Since n is in turn correlated with the degree of average Cu/Fe disorder, such prediction explains well the behavior reported for the $YBaCuFeO_5$ samples prepared with different cooling rates[21]. However, it is difficult to conciliate with the huge T_{spiral} changes observed in the $YBa_{1-x}Sr_xCuFeO_5$ and $ReBaCuFeO_5$ families, where the Cu/Fe disorder was kept approximately constant. A similar situation is observed with a second prediction, namely, the existence of a proportionality law between T_{spiral} and q_G. Such linear law should be verified by samples with different degrees of disorder, and this is indeed the case for the $YBaCuFeO_5$ series prepared with different cooling rates[21] (blue full circles in Fig. 4). More intriguing is the fact that the very same law is also verified by the $YBa_{1-x}Sr_xCuFeO_5$ (green full pentagons) and $ReBaCuFeO_5$ families (red full squares), and even by the $YBaCuFeO_5$ single crystal from ref. 29 (black star) to a very good approximation. This unexpected observation cannot be explained within the framework of the RFB model, and calls for the explicit consideration of lattice's impact in the different magnetic exchanges.

A third point needing further theoretical work is the origin of the intersection of T_{spiral} and $T_{collinear}$ for $q_G \sim 0.18$, and the sudden replacement of the spiral state by a second commensurate antiferromagnetic phase beyond this point. Given that it coincides with the smallest d_2 (i.e., largest J_{c2}) values of our study, the disappearance of the spiral

could be tentatively ascribed to the point where the AFM couplings between Fe-Fe impurities overcome the FM coupling of the bipyramids occupied by Cu-Fe pairs. The result would be a magnetic structure were all NN couplings are AFM, in agreement with the observation of the new magnetic propagation vector $\mathbf{k_{c'}} = $ (½ ½ 0). However, it is not clear why this point should coincide with the intersection of the $T_{collinear}$ and T_{spiral} lines. Another intriguing observation is the continuous evolution of the spiral-to-collinear phase transition from 2nd to 1st ordering by approaching the paramagnetic-collinear-spiral triple point. Information about the behavior of the different magnetic phases beyond the crossing of the $T_{collinear}$ and T_{spiral} lines should help to understand its exact nature, and in particular, to clarify whether we could be in presence of a Lifschitz point[35, 36]. We note also that its increased entropy at the crossing makes this point potentially interesting for the search of exotic magnetic states in presence of external perturbations such as magnetic fields or elevated pressures[35, 37, 38].

Towards spiral design in layered perovskites

An important outcome of the structural property correlations presented in previous sections is that they enable to propose a simple set of rules for the design of high-temperature spin-spirals in other AA'BB'O$_5$ layered perovskites with B-site disorder. Besides maintaining electric neutrality, the most critical point is to identify B/B' cation pairs of comparable sizes, affinity for square-pyramidal coordination, able to produce weak, alternating FM and AFM couplings along c-axis, and with a *very* large value for *one* of the two J_{BB} or $J_{B'B'}$ couplings. The choice is mostly limited by the relatively small number of pairs resulting in FM coupling within the pyramids, but among 3d transition metals, Cu^{2+}/Cu^{3+}, Cu^{2+}/Co^{3+}(high-spin) , Cu^{2+}/Mn^{3+} or Mn^{2+}/Co^{3+}(low-spin) could be

possible candidates if J_{BB} and $J_{B'B'}$ have the appropriate absolute values. DFT estimations of the magnetic exchanges, in particular for 4d and 5d pairs, will be highly desirable, and shall increase the number of potential candidates. The choice of the A/A'-cations requires ionic radii different enough to stabilize the layered perovskite structure. However, the highest T_{spiral} values can be achieved when the ionic radius of the A-cation close to the apical oxygen is small, and the $r^A_{ionic} - r^{A'}_{ionic}$ difference as small as possible (Fig. 5). Concerning thin film design, we saw that $c/2a$ alone is not a good parameter for T_{spiral} control. Hence, high T_{spiral} values can be a priori stabilized under both, tensile or compressive strain as long as the rules concerning the choice of the A and B cations are fulfilled.

We can also speculate on the expected behavior of T_{spiral} under external pressure. According to our findings, this will depend on the behavior of d_1/d_2, i.e., on the relative compressibility of these two distances. In general, bonds involving cations with high coordination or low valence expand or compress faster than those with cations in low coordination or with high valence[39, 40]. d_2, involving 12 (Ba^{2+}-O^{2-}) bonds, is thus expected to compress faster than d_1, where only 8 (R^{3+}-O^{2-}) bonds contribute. Since this will result in a smaller d_1/d_2 ratio, a decrease of T_{spiral} is thus predicted under the application of external pressure.

To summarize, we have experimentally validated an emerging route for stabilizing spin spirals up to temperatures far beyond RT. Our approach, based in the combination of chemical disorder with a targeted lattice tuning of some magnetic exchanges, takes full advantage of the additivity of these two mechanisms. As a result, the stability domain of the spiral magnetic order can be tuned over unprecedentedly large temperature ranges.

In the particular case of Cu/Fe-based layered perovskites we demonstrate that T_{spiral} values close to 400 K can be reached using this strategy. This value is ~100 K higher than using chemical disorder alone[21], and comfortably far beyond RT. We also reveal the existence of a linear, universal relationship between the spiral's ordering temperature and periodicity, a paramagnetic–collinear-spiral triple point, as well as several correlations between the spiral properties and some structural parameters. We discuss these results on the light of a recently proposed random frustrating bonds based mechanism, and propose a simple set of rules for the design of magnetic spirals in isostructural layered perovskites by using external pressure, chemical substitutions or epitaxial strain. Besides overcoming one of the main stoppers for applications, these results could accelerate the discovery of other materials featuring spiral phases stable well beyond RT, paving the way towards the long-sought technological use of magnetic spirals in spintronics devices.

Materials and Methods

Materials synthesis

The ReBaCuFeO$_5$ and YBa$_{1-x}$Sr$_x$CuFeO$_5$ polycrystalline samples were prepared using the solid state reaction method. High-purity Re$_2$O$_3$ or Y$_2$O$_3$ (99.995 - 99.998%, Aldrich / Alfa Aesar), SrCO$_3$ (99.995%, Aldrich), BaCO$_3$ (99.997%, Alfa Aesar), CuO (99.995%, Alfa Aesar) and Fe$_2$O$_3$ (99.998%, Alfa Aesar) powders were used as starting materials. Dehydrated rare-earth oxide powders were obtained by heating them at 1223 K for 15 hours. The required stoichiometric amounts of Re$_2$O$_3$, SrCO$_3$, BaCO$_3$, CuO and Fe$_2$O$_3$ were then weighted, thoroughly ground and heated at a rate of 300 K/h up to the synthesis temperature T_s (= 1323 – 1430 K), that was optimized for every sample using

thermogravimetric analysis under He/O_2 gas flow. The powders were then annealed during 50 hours at this temperature under oxygen gas flow. The obtained materials were cooled in the furnace down to RT, thoroughly grounded again, pressed into pellets, and sintered at T_s for another 50 hours. After this treatment, all samples were quenched into liquid nitrogen. Small pieces were kept solid for their use in magnetization measurements, and the rest was pulverized and subsequently employed in PND experiments. The phase purity of all samples was checked using laboratory powder x-ray diffraction (XRD) at RT using a Brucker D8 Advance diffractometer with Cu K_α radiation. All samples were very well crystalized and free of impurities within the limit of this technique (~1%).

Magnetic susceptibility

DC magnetization (M) measurements were performed in a superconducting quantum interference device magnetometer (MPMS-XL 7T, Quantum Design). Small pellets ($D \sim$ 3 mm, $H \sim$ 1 mm, $m \sim$ 15-25 mg) from the same batches as the samples used for the PND measurements were measured between 2 and 400 K by heating under a magnetic field of $\mu_0 H = 0.5$ T after being cooled down to 2 K in zero field. The magnetization was further measured between 300 and 600 K using a high temperature insert. The samples, mounted on transparent drinking straws for the measurements below 400 K, were dismounted and wrapped in aluminum foil as described in ref. 41 for the measurements above this temperature. The signal from the aluminum foil, measured separately, was found to be temperature-independent and negligible when compared with the sample's magnetization. For the samples with magnetic Re^{3+} cations, the magnetic transitions from Cu/Fe sublattice are difficult to observe in the magnetization data due the large paramagnetic contribution of the Re^{3+} moments, and they have been

missed in some previous studies[42]. However, they can still be tracked in the first derivatives of the DC inverse susceptibility $1/\chi^{DC}$ = H/M (fig. S1). The values of $T_{collinear}$ and T_{spiral} derived from this technique correspond to the midpoint of the step-like anomalies in the $1/\chi^{DC}$ derivative, which coincides with the χ^{DC} maximum in $YBa_{1-x}Sr_xCuFeO_5$ series.

It is worth mentioning that, although the $ReBaCuFeO_5$ samples investigated in this work were also synthesized in the past[43, 44], the existence of magnetic transitions has only been reported for a few of them[42, 45, 46, 47, 48], and there is no apparent systematics between the reported ordering temperatures and the Re ionic radii. A similar situation was observed in the $YBa_{1-x}Sr_xCuFeO_5$ series, where the presence of spiral phases was either disproven[49], or not demonstrated[50] in previous works. As shown in Fig. 2C, this is not the case in this study, where the collinear and spiral phases are clearly observed for *all* samples. Moreover, $T_{collinear}$ and T_{spiral}, change in a monotonic way as a function of both, the Re ionic radius and the Sr content x.

Differential scanning calorimetry

The paramagnetic to collinear phase transition at $T_{collinear}$ was also measured by differential scanning calorimetry (DSC) for $ReBaCuFeO_5$ and $YBa_{1-x}Sr_xCuFeO_5$ powder samples by using a NETZSCH DSC 204F1 device. Fine powders (~ 30 mg mass) were sealed into aluminum crucibles and heated up to 670 K with a rate of 15 K/min under Ar gas flow. The data were acquired during the heating process (see fig. S2).

Powder neutron diffraction

Powder neutron diffraction measurements were carried out at the Swiss Neutron Source SINQ of the Paul Scherrer Institute in Villigen, Switzerland, and the Institut Laue-Langevin in Grenoble, France. The $ReBaCuFeO_5$ and $YBa_{1-x}Sr_xCuFeO_5$ powder samples were introduced in cylindrical vanadium cans with (D = 6 mm, H = 5 cm) and mounted on the stick of a helium cryostat (2 - 300 K) and a cryofurnace (2 - 500 K). PND patterns were continuously recorded at the powder diffractometer DMC (Pyrolitic Graphite (002), λ = 2.458 Å and λ = 4.507 Å, $2\theta_{step}$ = 0.1°) while ramping the temperature from 10 to 480 K. Longer acquisitions for magnetic structure refinements were made at 10 K. High resolution patterns at both 10 K and 300 K were also recorded at the powder diffractometer HRPT (Ge (822), $2\theta_{step}$ = 0.05°, λ = 1.154 Å) and D2B (Ge (335), $2\theta_{step}$ = 0.05°, λ = 1.594 Å). The wavelengths and zero offsets were determined using a NAC reference powder sample. In the case of $DyBaCuFeO_5$ the impact of the relatively large neutron absorption cross section of natural dysprosium (994(13) barn) in the data was corrected by including in the refinements the μR values determined experimentally for the different wavelengths. The background from the sample environment was minimized through 5' collimators (D2B), and an oscillating radial collimator (HRPT). The values of $T_{collinear}$ and T_{spiral} derived from this technique correspond respectively, to the set-up and the maximum of the magnetic Bragg reflection (½ ½ ½), that roughly coincide with the values determined from χ^{DC} and DSC (see figs. S1 and S2, tables S1 and S2).

Data analysis

All diffraction data were analyzed using the Rietveld package FullProf Suite[51]. The structural refinements for $ReBaCuFeO_5$ were carried out by combing both HRPT and D2B data sets recorded at room temperature and 10 K. For $YBa_{1-x}Sr_xCuFeO_5$, HRPT

data recorded at room temperatures and 10 K were used for the fits of the crystal structure (fig. S6). The magnetic refinements were performed on DMC data recorded at 10 K by fixing the structural parameters as determined from refinements of HRPT and D2B patterns (fig. S4). We used the non-centrosymmetric space group *P4mm* for the description of the crystal structure. The choice was motivated by the fact that, contrarily to the centrosymmetric space group *P4/mmm*, *P4mm* enables to refine the occupation of the split Cu and Fe sites.

The Cu/Fe disorder was described by splitting the atomic position (½ ½ z) inside of the two pyramidal sites of the unit cell as shown in the tables S3 to S6. In the fully disordered case both positions are equally occupied in all pyramids (i.e., n_{Fe} = n_{Cu} = 50%), whereas full Cu/Fe order corresponds to n_{Cu} = 100%, n_{Fe} = 0 (or n_{Cu} = 0, n_{Fe} = 100%). As shown in tables S3 to S6, the samples investigated in this work are very close to the first scenario, i.e., of $|n_{Cu} - n_{Fe}|$ very close to zero. Note that Rietveld fits are not sensible to occupational correlations. The Cu/Fe disorder is thus assumed to be random, and the refined n_{Cu} and n_{Fe} *values* represent the average values over the full sample.

Anisotropic Debye-Waller factors were used for all atoms with exception of Y/Re (nearly isotropic, see ref. 21), Cu and Fe. The z coordinates of the two basal oxygen sites O2 and O2' were refined separately but their mean-square displacements (MSD) were restricted to have the same value (tables S4 to S6). No signature of interstitial oxygen at the (½, ½, z) atomic position could be observed, indicating that deviations from the sample's formula stoichiometry, if any, were within the detection limit of PND in all the samples investigated. For the $YBa_{1-x}Sr_xCuFeO_5$ sample with x = 0.5 we could not find

any evidence of alternating Ba/Sr layers, recently predicted for $x \geq 0.5$[26] and easy to identify due to the associate doubling of the *c* lattice parameter.

The collinear and spiral magnetic structures were described according to the models reported in ref. 18. The best fits obtained at 10 K for all samples are shown in fig. S4. The ratio between the $Fe^{3+}(3d^5$ HS) and Cu^{2+} $(3d^9)$ magnetic moments was restricted to be the same than their free ion, spin-only values (5:1). In the temperature regions where the collinear and spiral phases coexist, the Fe and Cu magnetic moments were restricted to have the same value and the same inclination with respect to the *ab*-plane in the two magnetic phases.

References and Notes

1. S. T. Bramwell, M. J. P. Gingras, Spin ice state in frustrated magnetic pyrochlore materials. *Science* **294**, 1495 (2001).

2. S. Gao, O. Zaharko, V. Tsurkan, Y. Su, J. S. White, G. S. Tucker, B. Roessli, F. Bourdarot, R. Sibille, D. Chernyshov, T. Fennell, A. Loidl, Ch. Rüegg, Spiral spin-liquid and the emergence of a vortex-like state in $MnSc_2S_4$. *Nat. Phy.* **13**, 157 (2017).

3. L. Balents, Spin liquids in frustrated magnets. *Nature* **464**, 199 (2010).

4. T. Fennell, *P. P. Deen, A. R. Wildes, K. Schmalzl, D. Prabhakaran, A. T. Boothroyd, R. J. Aldus, D. F. McMorrow, S. T. Bramwell,* Magnetic Coulomb Phase in the Spin Ice $Ho_2Ti_2O_7$. *Science* **326**, 415 (2009).

5. R. Sibille, E. Lhotel, M. C. Hatnean, G. J. Nilsen, G. Ehlers, A. Cervellino, E. Ressouche, M. Frontzek, O. Zaharko, V. Pomjakushin, U. Stuhr, H. C. Walker, D. T. Adroja, H. Luetkens, C. Baines, A. Amato, G. Balakrishnan, T. Fennell, M.

Kenzelmann, Coulomb spin liquid in anion-disordered pyrochlore $Tb_2Hf_2O_7$. *Nat. Commun.* **8**, 892 (2017).

6. E. S. Dreier, S. L. Holm, K. Lønbæk, U. B. Hansen, M. Medarde, I. Živković, P. Babkevich, M. Ruminy, N. Casati, A. Piovano, S. Rols, G. J. Nilsen, M. Boehm, M. Skoulatos, J. Schefer, H. M. Rønnow, T. Fennell, and K, Lefmann 24-spin clusters in the mineral boleite $KPb_{26}Ag_9Cu_{24}Cl_{62}(OH)_{(48)}$. *Phys. Rev. B*, **97**, 014416 (2018).

7. S. Mühlbauer, B. Binz, F. Jonietz, C. Pfleiderer, A. Rosch, A. Neubauer, R. Georgii, P. Böni, Skyrmion Lattice in a Chiral Magnet. *Science* **323**, 915 (2009).

8. B. Thielemann, Ch. Rüegg, H. M. Rønnow, A. M. Läuchli, J.-S. Caux, B. Normand, D. Biner, K. W. Krämer, H.-U. Güdel, J. Stahn, K. Habicht, K. Kiefer, M. Boehm, D. F. McMorrow, J. Mesot, Direct Observation of Magnon Fractionalization in the Quantum Spin Ladder. *Phys. Rev. Lett.* **102**, 107204 (2009).

9. J. S. White, T. Honda, K. Kimura, T. Kimura, Ch. Niedermayer, O. Zaharko, A. Poole, B. Roessli, M. Kenzelmann, Coupling of Magnetic and Ferroelectric Hysteresis by a Multicomponent Magnetic Structure in Mn_2GeO_4. *Phys. Rev. Lett.* **108**, 077204 (2012).

10. L. C. Chapon, G. R. Blake, M. J. Gutmann, S. Park, N. Hur, P. G. Radaelli, S-W. Cheong, Structural anomalies and multiferroic behavior in magnetically frustrated $TbMn_2O_5$. *Phys. Rev. Lett.* **93**, 177402 (2004).

11. N. J. Perks, R. D. Johnson, C. Martin, L. C. Chapon, P. G. Radaelli, Magneto orbital helices as a route to coupling magnetism and ferroelectricity in multiferroic $CaMn_7O_{12}$. *Nat. Commun.* **3**, 1277 (2012).

12. T. Kimura, T. Goto, H. Shintani, K. Ishizaka, T. Arima, Y. Tokura, Magnetic control of ferroelectric polarization. *Nature* **426**, 55 (2003).

13. N. A. Spaldin, M. Fiebig, The renaissance of magnetoelectric multiferroics.

Science **309**, 391 (2005).

14. M. Kenzelmann, A. B. Harris, S. Jonas, C. Broholm, J. Schefer, S. B. Kim, C. L. Zhang, S.-W. Cheong, O. P. Vajk, and J. W. Lynn, Magnetic inversion symmetry breaking and ferroelectricity in $TbMnO_3$. *Phys. Rev. Lett.* **95**, 087206 (2005).

15. H. Katsura, N. Nagaosa, A. V. Balatsky, Spin current and magnetoelectric effect in noncollinear magnets. *Phys. Rev. Lett.* **95**, 057205 (2005).

16. M. Mostovoy, Ferroelectricity in spiral magnets. *Phys. Rev. Lett.* **96**, 067601 (2006).

17. T. Kimura, Y. Sekio, H. Nakamura, T. Siegrist , A. P. Ramirez. *Nat. Mater.* **7**, 291. (2008).

18. Y. Tokura, S. Seki, N. Nagaosa, Multiferroics of spin origin. *Rep. Prog. Phys.* **77**, 076501 (2014).

19. T. Kimura. Magnetoelectric Hexaferrites. *Annu. Rev. Condens. Matter Phys.* **3**, 93 (2012).

20. M. Fiebig, T. Lottermoser, D. Meier, M. Trassin, The evolution of multiferroics. *Nat. Rev. Mater.* **1**, 16046 (2016).

21. M. Morin, E. Canévet, A. Raynaud, M. Bartkowiak, D. Sheptyakov, V. Ban, M. Kenzelmann, E. Pomjakushina, K. Conder, M. Medarde, Tuning magnetic spirals beyond room temperature with chemical disorder. *Nat. Commun.* **7**, 13758 (2016).

22. L. Er-Rakho, C. Michel, P. Lacorre, B. Raveau, $YBaCuFeO_{5+\delta}$: a Novel Oxygen-Deficient Perovskite with a Layer Structure. *J. Solid State Chem.* 73, 531 (1988).

23. Y. K. Atanassova, V. N. Popov, G. G. Bogachev, M. N. Iliev, C. Mitros, V. Psycharis, M. Pissas, Raman-Active and Infrared-Active Phonons in $YBaCuFeO_5$-Experiment and Lattice-Dynamics. *Phys. Rev. B* **47**, 15201 (1993).

24. M. Morin, A. Scaramucci, M. Bartkowiak, E. Pomjakushina, G. Deng, D.

Sheptyakov, L. Keller, J. Rodriguez-Carvajal, N. A. Spaldin, M. Kenzelmann, K. Conder, M. Medarde, Incommensurate magnetic structure, Fe/Cu chemical disorder, and magnetic interactions in the high-temperature multiferroic YBaCuFeO$_5$, *Phys. Rev. B* **91**, 064408 (2015).

25. R. D. Shannon, Revised effective ionic radii and systematic studies of interatomic distances in halides and chalcogenides. *Acta. Crystallogr. A* **32**, 751 (1976).

26. D. Dibyendu, S. Nandy, T. Maitra, C.S. Yadav, A. Taraphder, Nature of spiral state and absence of electric polarisation in Sr-doped YBaCuFeO$_5$ revealed first principle study. *Sci. Rep.* **8**, 2404 (2018).

27. A. W. Mombru, C. Christides, A. Lappas, K. Prassides, M. Pissas, C. Mitros, D. Niarchos, Magnetic-Structure of the Oxygen-Deficient Perovskite YBaCuFeO$_{5+\delta}$. *Inorg. Chem.* **33**, 1255 (1994).

28. V. Caignaert, I. Mirebeau, F. Bourée, N. Nguyen, A. Ducouret, J.-M. Greneche, B. Raveau, Crystal and Magnetic-Structure of YBaCuFeO$_5$. *J. Solid State Chem.* **114**, 24 (1995).

29. Y. C. Lai, C. H. Du, C. H. Lai, Y. H. Liang, C. W. Wang, K. C. Rule, H. C. Wu, H. D. Yang, W. T. Chen, G. J. Shu, Magnetic ordering and dielectric relaxation in the double perovskite YBaCuFeO$_5$. *J. Phys. Condens. Matter* **29**, 145801 (2017).

30. M. J. Ruiz-Aragón, E. Morán, U. Amador, J. L. Martínez, N. H. Andersen, and H. Ehrenberg, Low-temperature magnetic structure of YBaCuFeO$_5$ and the effect of partial substitution of yttrium by calcium. *Phys. Rev. B* **58**, 6291 (1998).

31. A. W. Mombru, K. Prassidesddag, C. Christidesddag, R. Erwin, M. Pissas, C Mitros, D. Niarchos, Neutron powder diffraction study (T=4.2-300K) and polarization analysis of YBaCuFeO$_{5+\delta}$. *J. Phys. Condens. Matter* **10**, 1247(1998).

32. A. Scaramucci, H. Shinaoka, M. V. Mostovoy, M. Müller, C. Mudry, M. Troyer, N. A.

Spaldin, Multiferroic Magnetic Spirals Induced by Random Magnetic Exchanges. *Phys. Rev. X* **8**, 011005 (2018).

33. A. Scaramucci, H. Shinaoka, M. V. Mostovoy, M. Müller, C. Mudry, Spiral order from orientationally correlated random bonds in classical XY models. arXiv: 1610. 00784.

34. Although the details of magnetic structure are still under debate, the only comparable example is the Néel temperature of the conical spiral phase in the hexaferrite $Sr_3Co_2Fe_{24}O_{41}$ (~ 400 K, see ref. 19). Although this material dies not display electric polarization at zero magnetic field, magnetoelectric effects have been observed a low magnetic fields.

35. R. M. Hornreich, M. Luban, S. Shtrikman, Critical Behavior at Onset of k-Space Instability on the $\lambda-$Line. *Phys. Rev. Lett.* **35**, 1678 (1975).

36. Y. Shapira, The Evidence for a Lifshitz Point in MnP. *J. Appl. Phys.* **53**, 1914 (1982).

37. T. Mazet, H. Ihou-Mouko, J. -F. Mareche, B. Malaman, Short-range magnetic order, irreversibility and giant magnetoresistance near the triple points in the (x, T) magnetic phase diagram of $ZrMn_6Sn_{6-x}Ga_x$. *Eur. Phys. J. B* **74**, 48 (2010).

38. R. M. Hornreich, M. Luban, S. Shtrikman, Critical Exponents at a Lifshitz Point to O(1/N). *Phys. Lett. A* **55**, 269 (1975).

39. M. Medarde, J. Mesot, P. Lacorre, S. Rosenkranz, P. Fischer, and K. Gobrecht, High-Pressure Neutron-Diffraction Study of the Metallization Process in $PrNiO_3$. *Phys. Rev. B* **52**, 9248 (1995).

40. M. Medardea, J. Mesot, S. Rosenkranz, P. Lacorre, W. Marshall, S. Klotz, J. S. Loveday, G. Hamel, S. Hull, P. Radaellif, Pressure-induced orthorhombic-rhombohedral phase transition in $NdNiO_3$. *Physica B* **234**, 15 (1997).

41. J. Sesé, J. Bartolomé, C. Rillo, Disposable sample holder for high temperature

measurements in MPMS superconducting quantum interference device magnetometers. *Rev. Sci. Instrum.* **78**, 046101 (2007).

42. S. Lal, K. Mukherjee, C. S. Yadav, Effect of crystalline electric field on heat capacity of LnBaCuFeO$_5$ (Ln = Gd, Ho, Yb). *Solid State Commun.* **270**, 130 (2018).

43. A. Klyndyuk, Thermoelectric properties of layered ferrocuprates LnBaCuFeO$_{(5+\delta)}$ (Ln= La, Pr, Nd, Sm, Gd-Lu). *Phys. Solid State* **51**, 250 (2009).

44. A. Klyndyuk, E. A. Chizhova, Structure and electrical and transport properties of cation-deficient samples of perovskite ferrocuprates RBaCuFe$_{5+\delta}$ (R = Y, La). *Phys. Solid State* **50**, 603 (2008).

45. Y. Kawamura, T. Kai, E. Satomi, Y. Yasui, Y. Kobayashi, M. Sato, K. Kakurai, High-Temperature Multiferroic State of RBaCuFeO$_5$ (R = Y, Lu, and Tm). *J. Phys. Soc. Jpn.* **79**, 073705 (2010).

46. A. W. Mombrúa, A. E. Goetab, H. Pardoa, P. N. Lisboa-Filhoc, L. Suescuna, R. A. Mariezcurrenaa, O. N. Venturad, R. Behaka, K. H. Andersene, F. M. Araújo-Moreiraf, Low-temperature magnetic properties of LuBaCuFeO$_{5+\delta}$ and TmBaCuFeO$_{5+\delta}$. *J. Solid State Chem.* **166**, 251(2002).

47. M. Kochi, J. Linden, T. Taniyama, K. Lehmus, M. Karppinen, H. Yamauchi, Magnetic properties, oxygen content and metal valences in BaRE(Cu$_{0.5}$Fe$_{0.5}$)$_2$O$_{5+\delta}$ with RE = Lu, Yb, Y, Eu, Sm, Nd and Pr. *Physica C* **338**, 132 (2000).

48. J. Linden, M. Kochi, K. Lehmus, T. Pietari, M. Karppinen, H. Yamauchi, Interplay between Cu and Fe valences in BaR(Cu$_{0.5}$Fe$_{0.5}$)O$_{5+\delta}$ double perovskites with R = Lu, Yb, Y, Eu, Sm, Nd, and Pr. *J. Solid. State Chem.* **168**, 354 (2002).

49. M. Pissas, G. Kallias, A. Simopoulos, D. Niarchos, E. Devlin, R. Sonntag, Mössbauer spectroscopy and neutron diffraction studies of the compound YSrCuFeO$_{5+y}$. *J. Phys. Condens. Matter* **10**, 10317 (1998).

50. S. Lal, S. K. Upadhyay, K. Mukherjee, C. S. Yadav, Evolution of magnetic and dielectric properties in Sr-substituted high-temperature multiferroic $YBaCuFeO_5$. *EPL.* **117**, 67066 (2017).

51. J. Rodriguez-Carvajal, Recent Advances in Magnetic-Structure Determination by Neutron Powder Diffraction. *Physica B* **192**, 55 (1993).

Figures

Fig. 1. Link between Cu/Fe chemical disorder and magnetic order in YBaCuFeO$_5$.

(A) Crystal structure of YBaCuFeO$_5$ with Cu/Fe disorder in the bipyramidal sites. **(B),** Schematic representation of the correlated Cu-Fe chemical disorder in YBaCuFeO$_5$, characterized by the presence of randomly-disordered Cu-Fe FM 'dimers'. **(C)** Magnetic structures of the commensurate collinear phase. J_{c1} and J_{c2} denote respectively the nearest neighbor AFM and FM couplings along the **c**-axis. **(D)** The representation of (B) in terms of weak, alternating AFM/FM bonds. The impact of a few, randomly distributed strong AFM Fe-Fe 'defects' is illustrated by the grey ellipses, which delimit the regions where the Cu-Fe spins loss their collinearity. The cross-talking of such regions eventually gives rise to a spiral if their separation is smaller than ξ_{min}. Note that the

same number of weakly interacting Cu-Cu defects is necessary in order to preserve the material's stoichiometry. The J-values are those of ref. 32 **(E)** Magnetic structure of the incommensurate spiral phase.
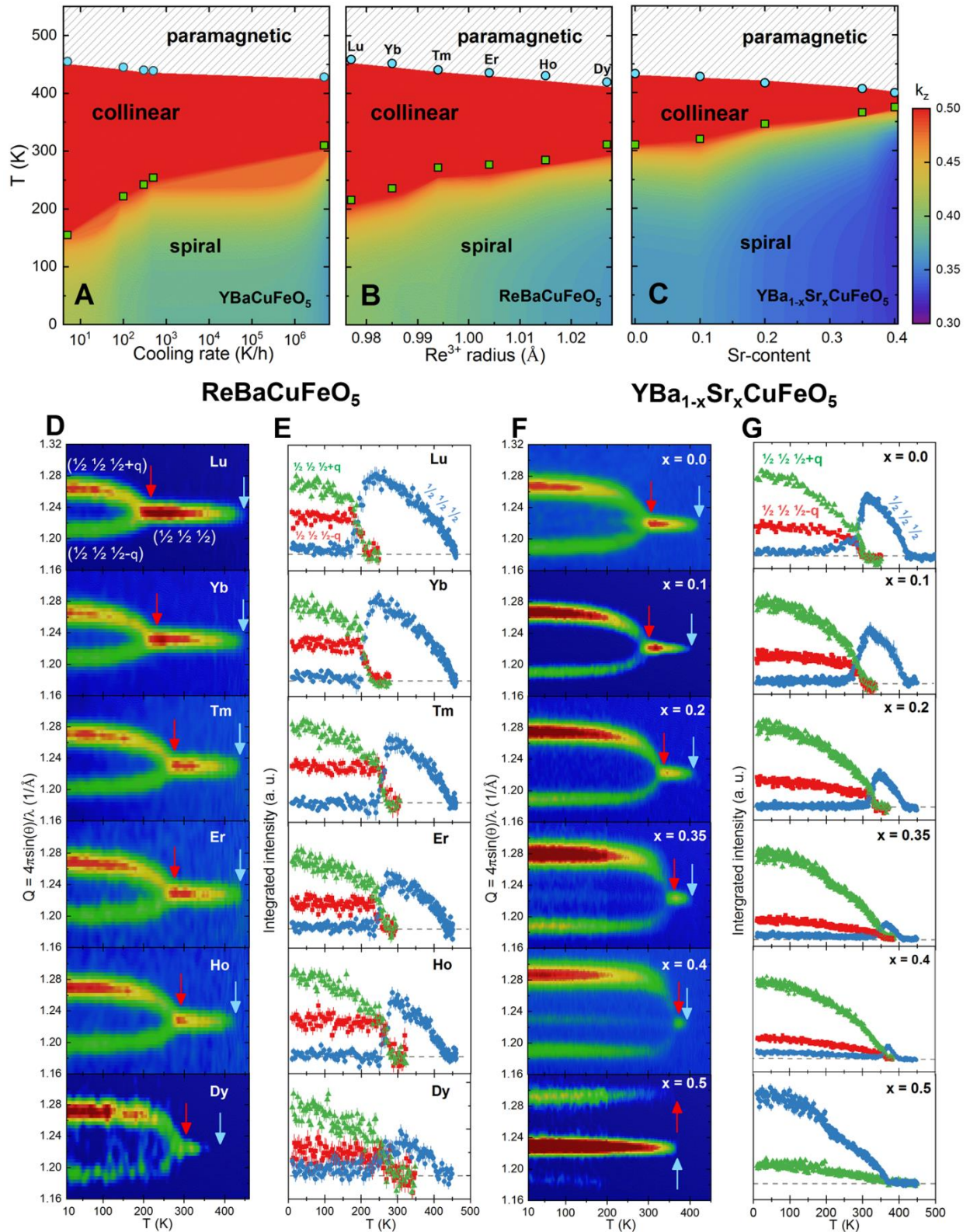
Fig. 2 Stability of the collinear and spiral phases with different tuning parameters. (A-C) Evolution of $T_{collinear}$ and T_{spiral} using different tuning parameters: (A) $YBaCuFeO_5$ prepared with different cooling rates (adapted from ref. 21); (B) Replacement of Y^{3+} by a rare-earth cation (Re^{3+}); (C) Replacement of Ba^{2+} by Sr^{2+}. The $T_{collinear}$ and T_{spiral} values are those determined from PND. The background color represents the z-component of magnetic propagation vector (k_z) which changes from ½ in the collinear phase to ½±q in the spiral phase (only ½-q is used in the figures). **(D-G)** Signature of the collinear and spiral phases in the PND patterns. The contour maps show the temperature dependence of the positions and the intensities of the commensurate (½ ½ ½) magnetic Bragg reflection and the incommensurate (½ ½ ½±q) satellites for the $ReBaCuFeO_5$ (D) and $YBa_{1-x}Sr_xCuFeO_5$ (F) series. The blue and red arrows indicate the ordering temperatures $T_{collinear}$ and T_{spiral}, respectively. The integrated intensities are shown in (E) for $ReBaCuFeO_5$, and (G) for $YBa_{1-x}Sr_xCuFeO_5$. For the Sr-doped sample with x = 0.5, the "minus" incommensurate satellites (½ ½ ½-q) was extremely weak (see also fig. S3). Hence, only the integrated intensity of the "plus" satellite (½ ½ ½+q) is shown. The error bars of the integrated intensities are the standard deviations obtained from 3-Gaussian least-square fits of the (½ ½ ½) Bragg reflection and its incommensurate satellites carried out using the Igor software.
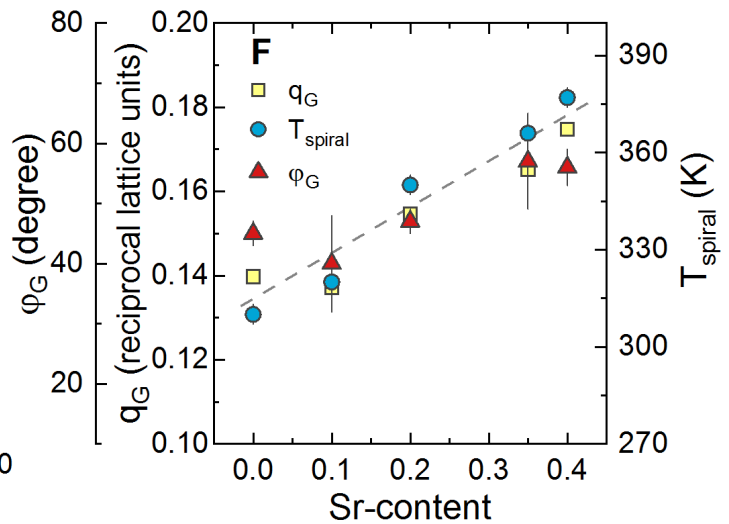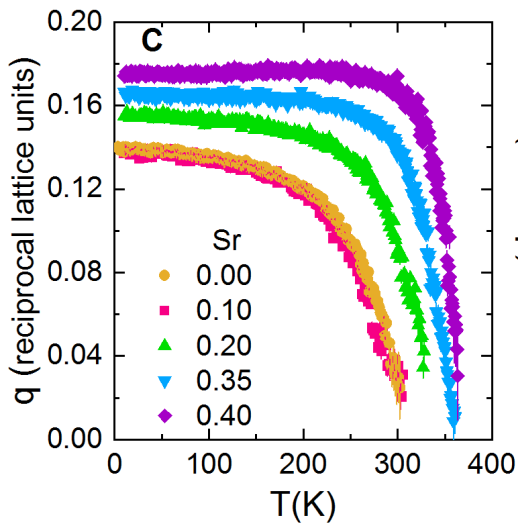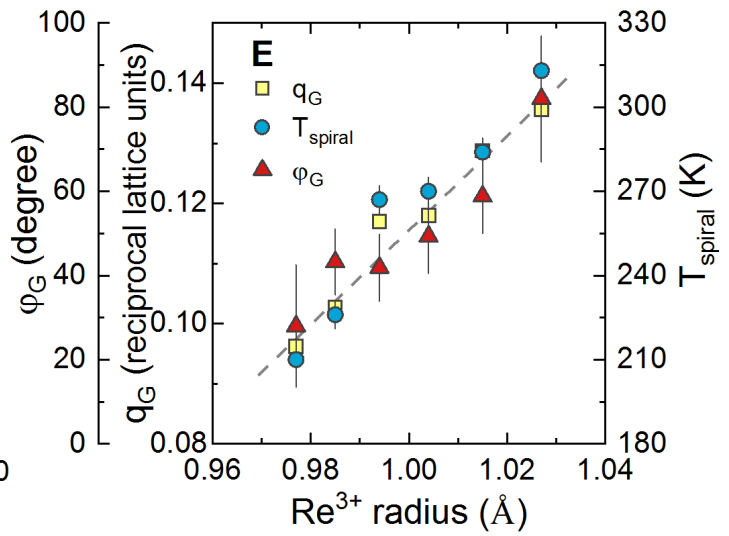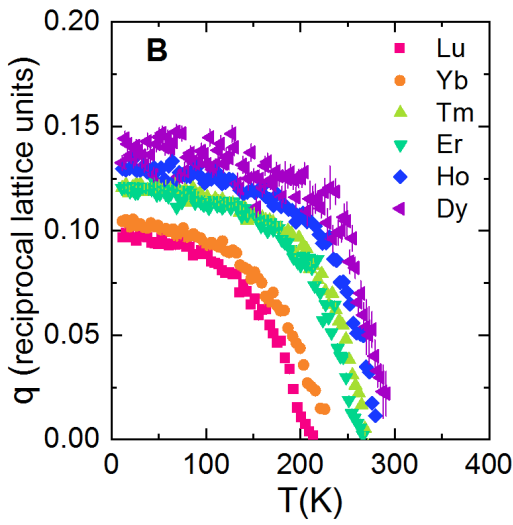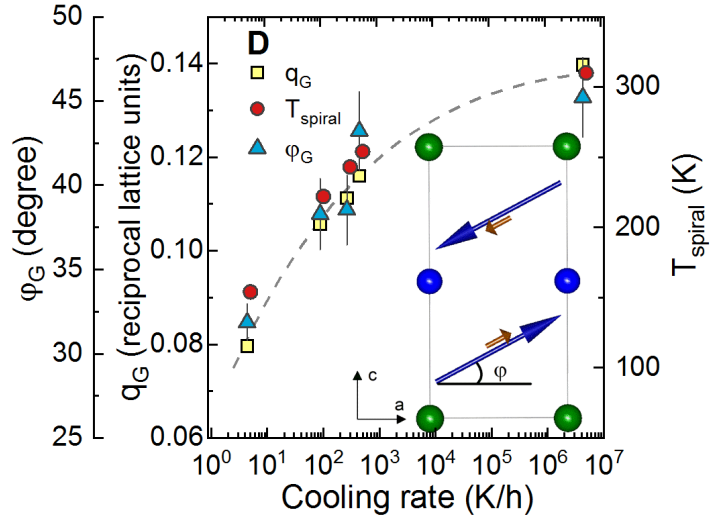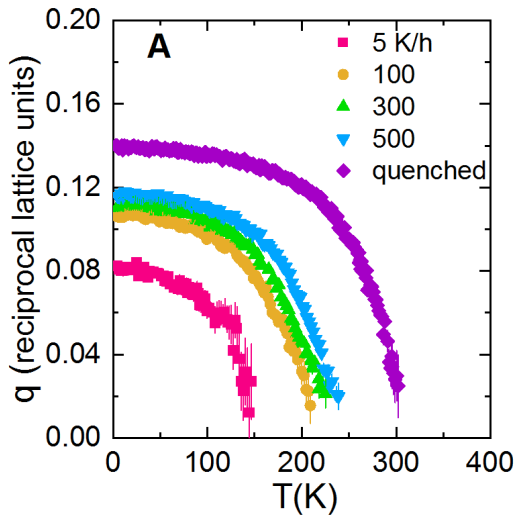
Fig. 3. Evolution of magnetic spiral properties with different tuning parameters.

(A-C) Temperature dependence of the magnetic modulation vector q in $YBaCuFeO_5$ using different tuning parameters: (A) Cooling rate (adapted from ref. 21). (B) Replacement of Y^{3+} by a rare-earth cation (Re^{3+}). (C) Replacement of Ba^{2+} by Sr^{2+}. **(D-F)** Evolution of T_{spiral} and the ground state values (10 K) of the magnetic modulation vector (q_G), and the inclination of the spiral rotation plane (φ_G) using different tuning parameters: (D) Cooling rate (adapted from ref. 21). (E) Replacement of Y^{3+} by a rare-earth cation (Re^{3+}). (F) Replacement of Ba^{2+} by Sr^{2+}. The inset in (D) shows the definition of the inclination angle φ_G. The dashed lines are guides for the eyes and indicate the positive correlation among T_{spiral}, q_G, and φ_G. The values of $ReBaCuFeO_5$ and $YBa_{1-x}Sr_xCuFeO_5$ families were extracted from Rietveld fits of the DMC data recorded at 10 K. The error bars of q_G and φ_G, listed in tables S3 and S4, are the standard deviations obtained from the fits of the magnetic structure using the FullProf Suite Rietveld package[51].
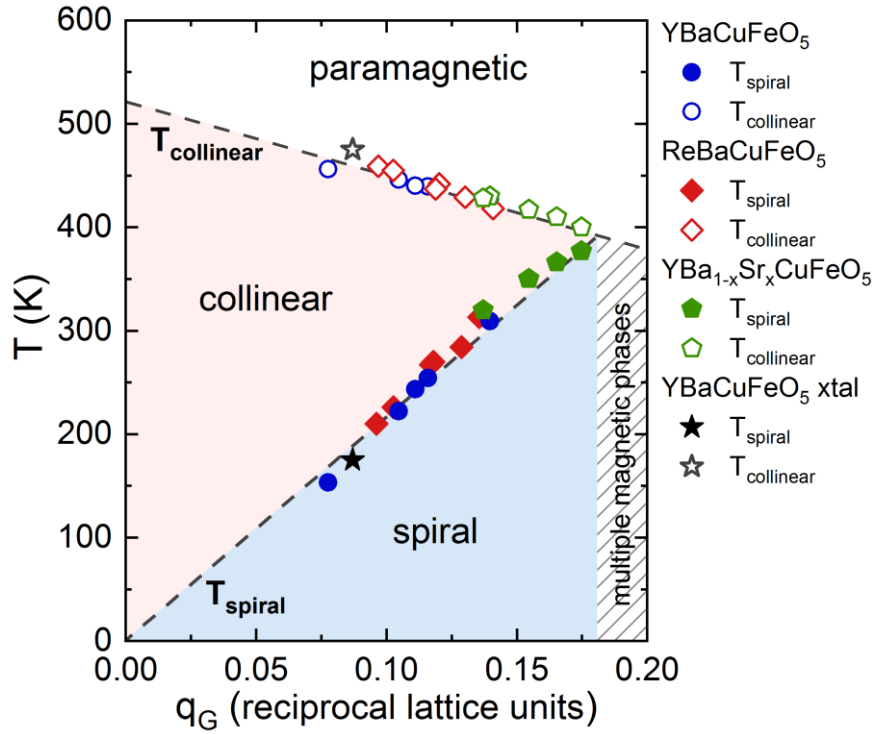
Fig. 4. Universal relationship between T_{spiral} and q_G in AA'CuFeO$_5$ layered perovskites. Correlation between T_{spiral} and the ground state magnetic modulation vector q_G in three families of AA'CuFeO$_5$ layered perovskites: YBaCuFeO$_5$ prepared with different cooling rates (full blue-symbols, data from ref. 21), ReBaCuFeO$_5$ with Re = Lu to Dy (full red-symbols), and YBa$_{1-x}$Sr$_x$CuFeO$_5$ with $0 \leq x \leq 0.5$ (full green-symbols). The full black star corresponds to the (q_G, T_{spiral}) point reported for a YbaCuFeO$_5$ single crystal in ref. 29. The $T_{collinear}$ values of all samples (open symbols) are also shown in order to illustrate its convergence with T_{spiral} at $q_G \sim 0.18$. The T_{spiral} and $T_{collinear}$ values are those determined from PND (tables S1 and S2). The error bars of q_G, listed in Supplementary tables S4 and S6, are the standard deviations obtained from the fits of the magnetic structure using the FullProf Suite Rietveld package[51], and they are smaller than the marker's size.
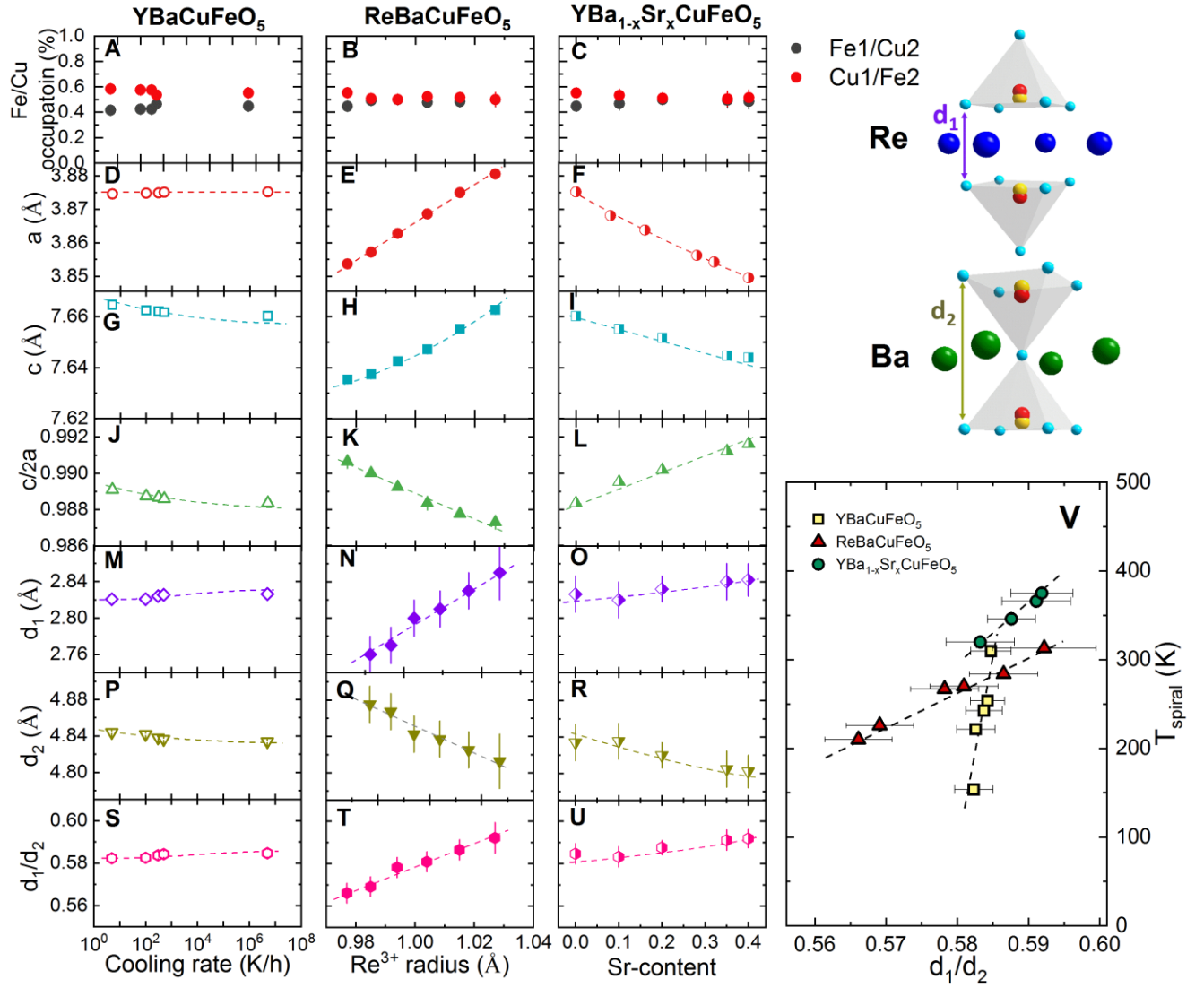
Fig. 5. **Link between crystal structure and magnetic ordering temperatures. (A-U)** Evolution of selected structural parameters as functions of the cooling rate ($YBaCuFeO_5$, data from ref. 21), the rare earth ionic radius ($ReBaCuFeO_5$), and the Sr content (x) ($YBa_{1-x}Sr_xCuFeO_5$). (A-C) Average Cu/Fe occupation in the pyramids. (D-I) Lattice parameters **a** and **c**. (J-L) Tetragonal distortion $c/2a$. (M-O) Distance d_1 between the bipyramidal layers along the **c**-axis. (P-R) Thickness d_2 of the bipyramidal layers. (S-U) d_1/d_2 ratio. **(V)** Evolution of T_{spiral} with d_1/d_2 ratio. The yellow, red, and green colors correspond respectively to $YBaCuFeO_5$ prepared with different cooling rates, $ReBaCuFeO_5$ (Re = Lu - Dy), and $YBa_{1-x}Sr_xCuFeO_5$ (x = 0 - 0.4). The T_{spiral} and $T_{collinear}$

values are those determined from PND (tables S1 and S2). The dashed lines are guides to the eyes. All structural parameters were extracted from the Rietveld fits of the high resolution PND data at RT (tables S3 and S5). The error bars are the standard deviations provided by the FullProf Suite Rietveld package[51].